TIR-ORQPM Technique for Generating Highly Efficient Second Harmonic

Moumita Saha and Sumita Deb

Abstract The generation of highly efficient second harmonic wavelength has been analyzed in this work by introducing the concept of optical rotation quasi-phase-matching technique by total-internal-reflection in yttrium oxide coated rectangular slab of magnesium oxide-doped lithium niobate crystal. At specific bounce sites inside the slab, the combined impact of optical rotation quasi-phase-matching and fractional quasi-phase-matching methods based on total-internal-reflection has resulted in highly improved conversion efficiency. The thin-film is introduced to regulate the phase-shifts caused by the propagation of *p*—and *s*-polarized light during total internal reflection at the slab-film interface. A graphical representation has been carried out using computer-aided simulation for a second harmonic wavelength of 514.5 nm while considering the effects of surface roughness, absorption and nonlinear law of reflection. Results show a peak conversion efficiency as high as 30.5%.

Keywords ORQPM · TIR · Electro-optic chiral · Second harmonic · Thin-film · Wave mixing · Underwater communication

1 Introduction

Over the last few years, quasi-phase-matching (QPM) technique has become a vital area of study. Many studies have indicated some popular methods for fabricating QPM waveguides, such as nonlinear material's periodic poling [1]. Fabrication error is the main weakness of this periodic poling approach [2], and it causes phase error between the interacting fields. This error results in a gradual decrease in the harmonic production [1, 2]. The revolution had taken place in 1962 when Armstrong et al. [3] presented the total-internal-reflection (TIR) based QPM technique which was carried forward by Boyd and Patel [4] as well as by Komine et al. [5] for second harmonic generation (SHG). The concept of fractional QPM was then introduced by Haïdar in

M. Saha (✉) · S. Deb
Department of Electrical Engineering, National Institute of Technology, Agartala, India
e-mail: er.moumitasaha@gmail.com

M. Tiwari et al. (eds.), *Optical and Wireless Technologies*, Lecture Notes in Electrical Engineering 892, https://doi.org/10.1007/978-981-19-1645-8_7

2005 [6]. Then, a surprising difference between the obtained results due to theoretical and experimental TIR-QPM technique has been addressed by Raybaut et al. in 2008 [7]. This difference is basically due to the destructive interference effect and had been explained by Bloembergen and Pershan's nonlinear law of reflection [8]. This destructive interference can be avoided by rotating the plane of polarization, according to Lewis Z. Liu et al. in 2012 and the concept is termed as optical rotation quasi-phase-matching (ORQPM) [9]. As per ref. [9], the efficiency of the circularly polarized harmonic generated by this ORQPM technique is approximately five times more efficient than the linearly polarized harmonics generated due to conventional QPM technique. Moreover, in 2012, L. Shi had demonstrated that, the polarization of an electro-optic (EO) chiral material can be controlled by the application of external electric field [10]. The conceptual accomplishment of this ORQPM approach has been compiled with the TIR phenomenon in our prior SHG study [11], third—and fourth-harmonic generation study [12], allowing polarization rotation controlled by an external electric field. In ref. [11], the ideal ORQPM condition cannot be achieved during SHG owing to the threshold limits of the crystalline slab under study. As a consequence, in this analysis, we attempted to minimize the deviation from the optimal ORQPM method as much as possible. The proposed frequency converter model requires a high level of flexibility in order to satisfy the QPM criterion while also triggering constructive interference of the produced light through polarization rotation without exceeding the allowable limits. Therefore, the concept of thin film used in ref. [11, 12] and [13] has also been incorporated here. The basic idea of this thin film inclusion had been described by Azzam in 1985 [14] and implemented in 2009 [15] for making the reflected light independent of polarization. The modified phase-shift equations during TIR for *p*-polarized (δ_{TP}) and *s*-polarized (δ_{TS}) light in presence of thin film have been considered for this numeric analytical work [11–13]

$$\delta_{TP} = \frac{4\pi}{\lambda} d_1 \left(N_1^2 - N_0^2 \sin^2 \varphi_0\right)^{1/2} - 2\tan^{-1} \frac{N_1^4 N_0 \cos\varphi_0 \sqrt{N_0^2 \sin^2 \varphi_0 - N_2^2}}{N_0^2 N_2^2 \left(N_1^2 - N_0^2 \sin^2 \varphi_0\right)} \quad (1)$$

$$\delta_{TS} = \frac{4\pi}{\lambda} d_1 \left(N_1^2 - N_0^2 \sin^2 \varphi_0\right)^{1/2} - 2\tan^{-1} \frac{N_0 \cos\varphi_0 \sqrt{N_0^2 \sin^2 \varphi_0 - N_2^2}}{\left(N_1^2 - N_0^2 \sin^2 \varphi_0\right)} \quad (2)$$

where, N_1 is the refractive index of thin film.

d_1 is the thin film thickness.

λ is the wavelength of the monochromatic incident light.

The incident angle φ_0 should be smaller than the light reflection critical angle of medium 0—medium 1 interface but greater than the light reflection critical angle of medium 0—medium 2 interface [15].

The light reflection critical angle at the medium 0—medium 1 interface is

$$\varphi_{C01} = \sin^{-1}\left(\frac{N_1}{N_0}\right) \quad (3)$$

The light reflection critical angle at the medium 0—medium 2 interface is

$$\varphi_{C02} = \sin^{-1}\left(\frac{N_2}{N_0}\right) \tag{4}$$

Therefore, the requisite for TIR at the medium 0—medium 2 interface, in the presence of medium 1(thin layer) is

$$\varphi_{C02} < \varphi_0 < \varphi_{C01} \tag{5}$$

And the provision for excluding TIR from the interface of the medium 0—medium 1, is [14]

$$N_0 \sin\varphi_0 < N_1 \tag{6}$$

As a result, the objective of this article is to give a better analysis of the ORQPM technique based on TIR by regulating the rotation period considerably closer to the ideal ORQPM scenario. The effect of surface roughness, absorption loss, and the interference effect of nonlinear law has been comprehended for SHG in this analysis.

2 Operational and Structural Analysis of Proposed Work

2.1 Geometrical Topology

Figure 1 portrays the geometrical topology of the proposed rectangular thin film coated semiconductor slab [11, 12].

Here, the crystal length is defined by L, crystal thickness by t, thin film thickness by d_1, bounce length by L_1 and the entry point of the driving radiation by X. The monocromatic light propagates through TIR and the optic axis is parallel to the horizontal plane.

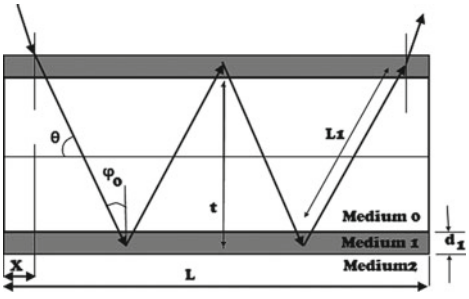

Fig. 1 Topology of semiconductor slab for the frequency conversion by ORQPM technique

2.2 Numeric-Analytical Study of the TIR-ORQPM Approach for SHG

The purpose of the proposed frequency converter is to generate highly efficient SH by the TIR-ORQPM technique in an EO chiral material under the influence of an external electric field. The ideal condition for ORQPM is $2L_c = 2L_r$, *i.e.*, the rotation period ($2L_r$) should be equal to double the coherence length. However, in our previous work of SHG [11], we were unable to fulfil this condition and settle down with a compromising state of $2\ L_c = 12L_r$ at a cost of efficiency drop. Therefore, the goal of this study is to achieve a near-optimal ORQPM condition while keeping the other variables within their allowable ranges. Here, the optical path length (L_B) and the external electric field (E) control the polarization rotation [10–12] as:

$$\beta = \frac{2}{\Lambda} \frac{\gamma_{51} E}{(1/n_e)^2 - (1/n_o)^2} L_B \tag{7}$$

where, Λ is the domain thickness, γ_{51} is EO coefficient for an applied external electric field along the y axis of MgO:LN crystal, n_e and n_o are the refractive indices of the extraordinary and ordinary wave respectively. Moreover, the bounce length (L_1) is regarded as domain thickness, Λ [11, 12]. The Eq. (7) is bounded with several conditions, such as the optical path length should be matched with the rotation period *i.e.,* $L_B = 2L_r$ and within this length, the condition of 2π polarization rotation has to be fulfilled as well. Therefore, to fulfill all the conditions while maintaining a proper slab thickness, the considered rotation period has to be eight times the coherence length *i.e.*, $2L_r = 8L_c$. Furthermore, the threshold limit of the applied electric field is maintained by considering the per bounce length as $\frac{8}{101}L_c$ *i.e.*, 101 bounces are required to rotate the polarization plane of the generated SH by 2π. Therefore, the SH field for ORQPM will be produced after every 101 bounces and that for fractional QPM at every bounce, as $L_1 = \frac{8}{101}L_c$. Consequently, the combined effect of ORQPM and fractional QPM is available after 101, 202, 303, 404, … bounces and so on. Here, the considered polarization configuration is *p*–*p*–*s* (type-I phase-matching) as it shows the lowest wave vector mismatch and thereby the generated harmonic field is *s*-polarized. This generated harmonic field is not aligned parallel to optic axis and hence the component wave (*p* and *s*) propagation has been considered for our mathematical analysis. This type of propagation generates an additional TIR phase-shift which affects the global phase-shift. Therefore, considering all the consequences, the generated harmonic field amplitude is written as [11]:

$$\text{For ORQPM}: A_{2\omega\_y(ORQPM)}(L_1) = 4\pi \left(\frac{2\omega}{n_{2\omega}c}\right) d_{pps} A_\omega^2 \left[\frac{2i\Delta k L_1 - e^{-i2\Delta k L_1} + 1}{4\Delta k}\right] \tag{8}$$

$$\text{For fractional QPM}: A_{2\omega\_y(Fractional QPM)}(L_1) = 4\pi\left(\frac{2\omega}{n_{2\omega}c}\right)d_{pps}A_{\omega}^{2}\left[\frac{1-e^{-i2\Delta kL_1}}{\Delta k}\right] \tag{9}$$

where $\Delta k = k_{2\omega} - 2k_{\omega}$, $n_{2\omega}$ is the optical index of the material for generated SH, A_{ω} represents the input beam field amplitude, $A_{2\omega}$ represents the generated beam field amplitude and the propagation direction is along the z-axis. For any intermediate length L_j, s-wave can be rewritten as [11]

For ORQPM: $A_{2\omega\_y\_s(ORQPM)}\left(L_j\right)$

$$= \left\{e^{-i(\Delta\varphi_1+\delta_{TS1})}\cos\theta + e^{-i(\Delta\varphi_2+2\delta_{TS2})}\cos^2\theta + \ldots + e^{-i(j-1)(\Delta\varphi_{(j-1)}+\delta_{TS(j-1)})}\cos^{(j-1)}\theta\right\}A_{2\omega\_y(ORQPM)}(L_1) \tag{10}$$

For fractional QPM: $A_{2\omega\_y\_s(Fractional QPM)}\left(L_j\right)$

$$= \left\{e^{-i(\Delta\varphi_1+\delta_{TS1})}\cos\theta + e^{-i(\Delta\varphi_2+2\delta_{TS2})}\cos^2\theta + \ldots + e^{-i(j-1)(\Delta\varphi_{(j-1)}+\delta_{TS(j-1)})}\cos^{(j-1)}\theta\right\}A_{2\omega\_y(Fractional QPM)}(L_1) \tag{11}$$

For any intermediate length L_j, p-wave can be rewritten as [11]

For ORQPM: $A_{2\omega\_y\_p(ORQPM)}\left(L_{j-1}\right)$

$$= \left\{e^{-i(\Delta\varphi_1+\delta_{TS1})}\sin\theta + e^{-i(\Delta\varphi_2+2\delta_{TS2})}\sin^2\theta + \ldots + e^{-i(j-1)(\Delta\varphi_{(j-1)}+\delta_{TS(j-1)})}\sin^{(j-1)}\theta\right\}A_{2\omega\_y(ORQPM)}(L_1) \tag{12}$$

For fractional QPM: $A_{2\omega\_y\_p(Fractional QPM)}\left(L_{j-1}\right)$

$$= \left\{\begin{array}{c} e^{-i(\Delta\varphi_1+\delta_{TS1})}\sin\theta + e^{-i(\Delta\varphi_2+2\delta_{TS2})}\sin^2\theta + \ldots \\ +e^{-i(j-1)(\Delta\varphi_{(j-1)}+\delta_{TS(j-1)})}\sin^{(j-1)}\theta \end{array}\right\}A_{2\omega\_y(Fractinal QPM)}(L_1) \tag{13}$$

As a result, the net SH electric field amplitude for n number of bounces as [11]: $A_{2\omega\_y}(L_1 + L_2 + L_3 + \ldots + L_n)$

$$= \sum_{j=1}^{n}\left\{\begin{array}{c} A_{2\omega_{y_{s(ORQPM)}}}\left(L_j\right) + A_{2\omega_{y_{s(Fractional QPM)}}}\left(L_j\right) \\ +A_{2\omega\_y\_p(ORQPM)}\left(L_{j-1}\right) + A_{2\omega\_y\_p(Fractional QPM)}\left(L_{j-1}\right) \end{array}\right\} \tag{14}$$

where n = 101, 202, 303, …

The net SH electric field $A_{2\omega\_y}$ is used to calculate the time-average SH intensity as:

$$I_{2\omega\_y} = \frac{n_{2\omega}c}{2\pi}\left|A_{2\omega\_y}\right|^2 \tag{15}$$

Finally, the SH peak conversion efficiency is determined by the combined field effect of ORQPM and the fractional QPM approach, as:

$$\eta_{SHG\_TIR-ORQPM\_fractional QPM} = \frac{I_{2\omega\_y}(z)}{I_p} \times 100\% \tag{16}$$

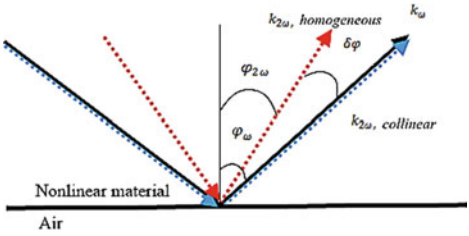

Fig. 2 Snell-Descartes law

I_p is the fundamental beam intensity assumed to be undepleted.

2.3 *Losses and the Interference Effect of the Nonlinear Law of Reflection*

A significant amount of efficiency drop is observed due to the absorption and roughness. The linear absorption coefficient α_ω is much less than 1 but its effect cannot be neglected. At each point of reflection, there is a reflection loss due to the surface roughness and is determined in terms of reflection coefficient R [16] (Fig. 2).

$$R \approx 1 - \left(\frac{4\pi n_j \sigma \cos\varphi_0}{\lambda_j}\right)^2 \tag{17}$$

where $j = \omega$ for the fundamental wave and $j = 2\omega$ for the generated SH, and σ is the standard deviation of surface roughness ($\sigma = p - v$ value/12) [16]. The p–v value is peak to valley value of the semiconductor's surface. However, the interference effect of the nonlinear law of reflection may cause destructive or even constructive outcome of interacting waves due to the non-collinearity effect of the generated homogeneous SH. According to reflection law of Bloembergen and Pershan [8], a nonlinear medium generates a collinear and a homogeneous SH field, which satisfies the Snell–Descartes law for a SHG situation:

$$N_\omega \sin\varphi_\omega = N_{2\omega} \sin\varphi_{2\omega} \tag{18}$$

The variation of angle between the generated homogeneous and generated collinear SH is:

$$\delta\varphi \approx -\frac{\delta N}{N} \tan\varphi_\omega \tag{19}$$

where $\delta N = N_{2\omega} - N_\omega$ is the optical dispersion and $N \approx N_\omega \approx N_{2\omega}$ [7].

3 Simulation Outcomes

3.1 Parameter Specification

The proposed scheme could be realized more precisely by the graphical representation of the simulation outcomes. The computer-aided simulation has been carried out by considering a crystal slab of 22 mm long (L), 125 μm (t) thick with a thin layer coating of 2.0 μm (d_1) for an incident angle of $\varphi_0 = 40°$, while the collimated optical beam entry point to the semiconductor slab is $X = 0.85$ mm (Fig. 1). The corresponding refractive indices of the chosen materials (MgO:LN and Y_2O_3) [11] have been estimated by the temperature dependent dispersion formula for the driving and generated radiations. The operating temperature (T) and the non-critical phase matching temperature (T_{ncpm}) are 300 K and 115 °C respectively. The period of rotation requires 64.79 kV/mm external electric which is less than the threshold limit of 65 kV/mm [17] for the chosen material. The input Gaussian beam having 100 μm waist, 100 mW power and *p–p–s* polarization is considered for the computer-aided simulation. The corresponding d-coefficient for the chosen polarization configuration can be expressed as [18]:

$$d_{pps} = d_{31} \sin\theta - d_{22} \cos\theta \sin 3\varphi \tag{20}$$

where θ is the angle between the wave vector and the optic axis, φ is the azimuthal angle and considered to be 90° for getting maximum effective d-coefficient value. The value of d_{31} and d_{22} for MgO:LN are considered to be 4.4 pm/V [18] and 6.6 pm/V [19] respectively. The absorption coefficient ($\alpha_\omega \approx \alpha_{2\omega}$), EO coefficient and the p–v value for MgO:LN are chosen to be 0.02 cm^{-1} [20], 0.96×10^{-5} cm/KV [19] and 6 nm [21].

3.2 Results Obtained for SHG on Y_2O_3 Coated MgO:LN Rectangular Slab

The equation for the conversion efficiency, considering the added field impact of TIR-ORQPM and fractional QPM technique, in Sect. 2.2, is for a loss less system without considering the nonlinear law of reflection. The recombinational effect of the nonlinear law of reflection shows significant impact on the conversion efficiency curve, which is also shown in Fig. 3. The recombinational effect is a combination of destructive and constructive interferences since the generated collinear SH field faces a 2 π phase-shift and the generated homogeneous SH field goes through different phase-shifts during TIR. The phase difference between the two mentioned SH field (collinear SH field and the homogeneous SH field) is nearly π after 35, 98, 162 bounces and the resultant field is fully destructive after these bounces. This destructive interference causes zero peak conversion efficiency at those particular bounce

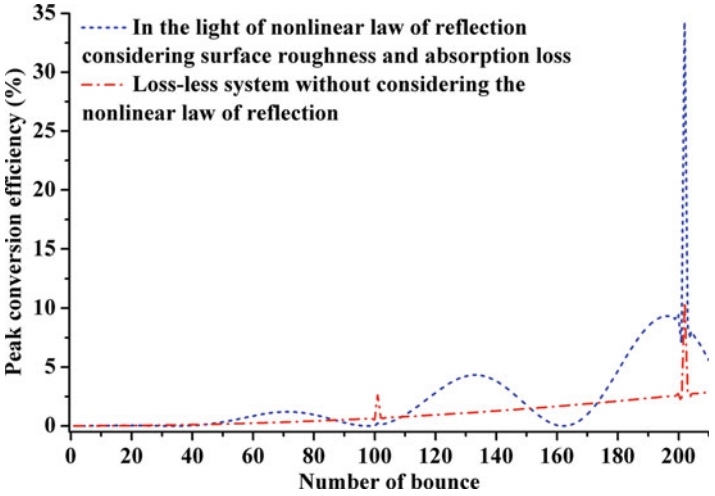

Fig. 3 Graphical representation of peak conversion efficiency vs number of bounce for SHG by TIR-ORQPM and fractional QPM technique **a** in the light of nonlinear law of reflection considering absorption and roughness **b** loss-less system without considering the nonlinear law of reflection

points, as shown in Fig. 3. After every destructive interference, there is a consistent decrement in the phase difference between the generated collinear and homogeneous SH field and a gradual increase in the peak conversion efficiency. Therefore, after the gradual decrease, the resultant SH field becomes constructive while the phase difference is zero *i.e.*, after 71, 133, 196 bounces, as shown in Fig. 3. However, the fractional QPM is occurred in every bounce and the ORQPM is taking place only at 101^{th} and 202^{th} bounces due to the polarization rotation of $2\ \pi$ as discussed in the 2.2 section. Hence, the combined field effect of the fractional QPM and ORQPM technique is appeared in 101^{th} and 202^{th} bounce and shows sudden peaks in the efficiency graph (Fig. 3). Moreover, a huge deviation has been observed between the most constructive point and the most efficient point as the interacting length plays an important role in this scenario. Now, considering all the circumstances (interacting length, added field effect and high constructive point), the simulation outcome shows the highest peak conversion efficiency point in Fig. 3.

3.3 Influence of Incident Angle

The angle of incidence is one of the most impactful controlling factors for global phase-shift, and its fluctuation causes a significant reduction in the efficiency, while the other operating and geometrical parameters are assumed to be unchanged. This decrease in efficiency is basically due to phase mismatch. Figure 4 shows the fluc-

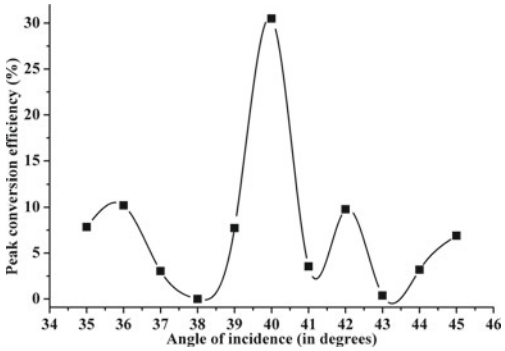

Fig. 4 Variation of peak conversion efficiency under the influence of incident angle

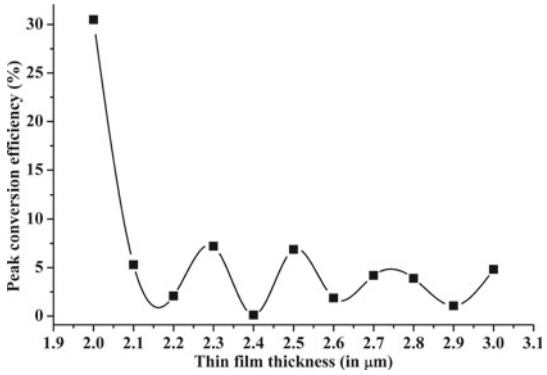

Fig. 5 Variation of peak conversion efficiency under the influence of thin film thickness

tuation of peak conversion efficiency w.r.t the incident angles and enunciate 40° as the most suitable one.

3.4 Affect of Thin Film Thickness

The thin film thickness plays an important role in the controlling of global phase-shift, and a slight variation causes a significant reduction in the peak conversion efficiency, while the other operating and geometrical parameters are constant. The reason behind this decrease is basically due to phase mismatch. Figure 5 shows the change of peak conversion efficiency w.r.t the thin film thickness and states 2.0 μm as the most suitable one.

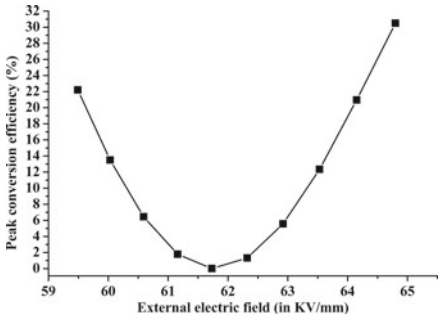

Fig. 6 Variation of peak conversion efficiency under the influence of external electric field

3.5 Influence of External Electric Field

The applied external electric field particularly controls the polarization rotation. As a result, if we alter the amplitude of the electric field, the rotation period will change accordingly, resulting in a variation in the peak conversion efficiency (Fig. 6). The period of rotation is 101, 102, 103, 104, 105, 106, 107, 108, 109, 110 for an external electric field of 64.79 kV/mm, 64.15 kV/mm¸ 63.53 kV/mm, 62.92 kV/mm, 62.32 kV/mm¸ 61.73 kV/mm, 61.16 kV/mm, 60.59 kV/mm¸ 60.03 kV/mm, 59.49 kV/mm respectively. However, Rayleigh range is maintained upto 210 bounces only. Hence, the rotation period at bounce no 106, 107, 108, 109 and 110 cannot be considered, as they violate the Rayleigh range during their second point of satisfying ORQPM condition and hence reflects low efficiency.

3.6 Influence of Input Power

A linear rise has been observed in the efficiency curve while increasing the input power as shown in Fig. 7.

3.7 Comparison Chart

Now, the reported SHG results can be compared with the proposed approach of achieving SHG. This comparison will help us to know that this process of SHG by TIR-based fractional QPM and ORQPM process has better performance in terms of peak conversion efficiency and fabrication complications (Table 1).

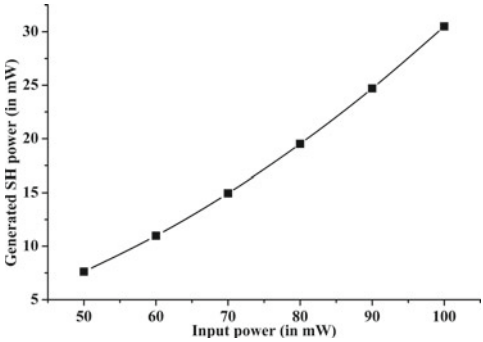

Fig. 7 Variation of peak conversion efficiency under the influence of input power

Table 1 Comparison of the proposed technique with the reported processes

Sl no	References	Efficiency	Phase-matching technique	Material used & its fabrication	Wavelength
1	[22]	0.2%	QPM	Periodically poled potassium niobate	926 nm (Fund)
2	[23]	16.5%	QPM	Periodically poled potassium niobate	488 nm (SH)
3	[24]	8%	QPM	Periodically poled lithium niobate thin-film wafer-bonded on silicon substrate and rib-loaded with silicon nitride channel	1580 nm (Fund)
4	[11]	32% (400 mW input power)	TIR based fractional & ORQPM	Rectangular slab of MgO doped LN crystal coated with a thin layer of Y_2O_3	532 nm (SH)
5	Proposed	30.50% (100 mW input power)	TIR based fractional & ORQPM	Rectangular slab of MgO doped LN crystal coated with a thin layer of Y_2O_3	514.50 nm (SH)

4 Discussions

The reported findings are specific to a given combination of structure, external electric field, operating temperature and wavelength. The proposed scheme outperforms conventional geometrical structures such as periodically polled or parallel (without thin film) slabs. The structural reconstruction of a parallel semiconductor slab generally used for the frequency conversion process has been accomplished by inserting

a thin coating on the surface, which has made it a favorable module for the TIR-ORQPM technique. This TIR-based ORQPM technique has already been realized in our previous work [11] for 532 nm SHG presenting 32% efficiency for 400 mW input power without fulfilling the ideal ORQPM condition and had to settle down with a conceding of efficiency drop for $2L_c = 12L_r$. Here, in this analysis we have tried to minimize this deviation from the ideal ORQPM condition and ended up with $2L_c = 8L_r$. There is a high chance of further improvement for more optimization of this rotation period. Furthermore, the frequency conversion process is dependent not only on the polarization rotation period but also on the phase-matching condition. This phase-matching condition is realized through the global phase-shift, which is controlled by the thin-film thickness. However, the polarization rotation is controlled by an external electric field. Variation of the material and thickness of the thin-film can build an immense effect on the global phase-shift of the interacting beams when travelling through TIR phenomenon and gives us an adequate facility to select suitable incident angle for further progression of our proposed scheme. The incident angle selection is the most crucial part of the proposed technique as it has to look after the electric field and operating temperature threshold limits. Moreover, the prime focus of this analytical approach is to improve the peak conversion efficiency without hampering the other parameters. A comparative conversion efficiency curve has been shown in Fig. 4 for a loss less system without considering the nonlinear law of reflection and a system in the light of nonlinear law of reflection considering absorption and reflection losses. The graphical representation of the outcome for 514.5 nm wavelength considering the limiting factors can signify the mathematical derivation of this paper demanding high efficiency. Thus, assuring high efficiency, this device is believed to be beneficial for underwater communications [25] and for medical applications as well [26]. Besides these applications, it can be used in laser lighting displays because of its flexibility in visible transmission window. The peak conversion efficiency obtained is 30.50% for 100 mW input power and shows much higher conversion efficiency than any other conventional QPM technique.

5 Conclusion

In conclusion, we may characterize the suggested scheme's topology as a thin-film coated (Y_2O_3) rectangular slab of MgO doped LN crystal and highlight its excellent peak conversion efficiency for the rotational phenomena of the polarization plane. This rotational phenomenon has been controlled by an external electric field. During the polarization rotation it is very difficult to satisfy the global phase-shift condition only by varying the incident angle and hence the thin-film concept has been incorporated. The proposed converter provides higher peak conversion efficiency in the visible spectrum range than the other conventional frequency converters. The nobility of this proposed scheme is the SHG by rotating the plane of polarization of the input radiation under the influence of a convenient external electric field across the semiconductor material. The chosen semiconductor material should flaunt circular

birefringence by the provocation of external electric field so that we can control the rotation of the polarization plane. This polarization rotation of the interacting beams along with the propagation distance is constant and the period of rotation should be equal to $2L_c$ for an ideal ORQPM situation. In the meantime, we have to look after the threshold limit of the other operating and the structural parameters. Therefore, we may need to compromise with the ideal ORQPM condition and settle for the $8L_c$ rotation period. This $8L_c$ period of rotation can be achieved after every 101 bounces by an external electric field of 64.79 kV/mm. It is clear from the graphical evaluation that a slight fluctuation in incident angle, thin-film thickness, and electric field can make a huge impact on peak conversion efficiency. The conversion yield-limiting elements are included in the computer-aided simulation and provide a peak conversion efficiency of 30.50% for an input power of 100 mW while generating 514.5 nm SH wavelength. Thus, by regulating the polarization rotation in a bulk EO chiral material, this extremely efficient frequency converter can effectively contribute to the phenomenon of TIR-based phase-matching phenomenon.

References

1. Magel GA, Fejer MM, Byer RL (1990) Quasi-phase-matched second-harmonic generation of blue light in periodically poled LiNbO3. Appl Phys Lett 56(2):108–110. https://doi.org/10.1063/1.103276
2. Fejer MM, Magel GA, Lim EJ (1990) Quasi-phase-matched interactions in lithium niobate. Edited by Howard R. Schlossberg and Raymond V. Wick, 213, San Diego. https://doi.org/10.1117/12.962160.
3. Boyd GD, Patel CKN (1966) Enhancement of optical second-harmonic generation (SHG) by reflection phase matching in ZnS and GaAs. Appl Phys Lett 8:313–315
4. Komine H, Long WH, Tully JW, Stappaerts EA (1998) Quasi-phase-matched second-harmonic generation by use of a total-internal-reflection phase shift in gallium arsenide and zinc selenide plates. Opt Lett 23:661–663
5. Haïdar R (2005) Fractional quasi-phase-matching by Fresnel birefringence. Appl Phys Lett 88:211102
6. Armstrong JA, Bloembergen N, Ducuing J, Pershan PS (1962) Interactions between light waves in a nonlinear dielectric. Phys Rev 127(6):1918–1939. https://doi.org/10.1103/PhysRev.127.1918
7. Raybaut M, Godard A, Toulouse A, Lubin C, Rosencher E (2008) Fresnel phase matching: exploring the frontiers between ray and guided wave quadratic nonlinear optics. Opt Express 16(22):18457. https://doi.org/10.1364/OE.16.018457
8. Bloembergen N, Pershan PS (1962) Light waves at the boundary of nonlinear media. Phys Rev 128(2):606–622. https://doi.org/10.1103/PhysRev.128.606
9. Liu Lewis Z, O'Keeffe Kevin, Hooker Simon M (2012) Optical rotation Quasi-Phase-matching for circularly polarized high harmonic generation. Opt Lett 37(12):2415. https://doi.org/10.1364/OL.37.002415
10. Shi L, Tian L, Chen X (2012) Electro-optic chirality control in MgO:PPLN. J Appl Phys 112:073103
11. Saha M, Deb S, Mandal PK, Medhi B, Saha A (2021) Highly efficient second-harmonic generation in an electro-optic chiral material using total-internal-reflection-based optical rotation quasi-phase-matching technique. Opt Eng 60(6):066104. https://doi.org/10.1117/1.OE.60.6.066104

12. Saha M, Deb S (in press) Highly efficient third and fourth harmonic generation using total-internal-reflection based optical rotation quasi-phase-matching. Phys Wave Phenom. Accessed on 13 Sept 2021
13. Saha M, Deb S, Medhi B, Barma MD (2020) Utilization of thin-film to control total phase shift during total-internal-reflection. In: 2020 IEEE international women in engineering (WIE) conference on electrical and computer engineering (WIECON-ECE). https://doi.org/10.1109/WIECON-ECE52138.2020.9398045
14. Azzam RMA (1985) Simultaneous reflection and refraction of light without change of polarization by a single-layer-coated dielectric surface. Opt Lett 10(3):107. https://doi.org/10.1364/OL.10.000107
15. Azzam RMA (2009) Total internal reflection without change of polarization using a right-angle prism with half-wavelength-thick optical interference coating. Opt Lett 34:371–373
16. Haïdar R, Forget N, Kupecek P, Rosencher E (2004) Fresnel phase matching for three-wave mixing in isotropic semiconductors. J Opt Soc Am B 21(8):1522. https://doi.org/10.1364/JOSAB.21.001522
17. Minet Y, Reis L, Szabados J, Werner CS, Zappe H, Buse K, Breunig I (2020) Pockels-effect-based adiabatic frequency conversion in ultrahigh-Q microresonators. Opt Express 28(3):2939–2947. https://doi.org/10.1364/OE.378112
18. Nikogosyan DN (2005) Nonlinear optical crystals: a complete survey. Springer, New York, p 163
19. Bonghoon K, Rhee BK, Joo G-T (2006) Variation of electro-optic coefficients in MgO-doped LiNbO3 single crystals. Mat Lett 60(17–18):2306–2308. https://doi.org/10.1016/j.matlet.2005.12.144
20. Schwesyg JR, Markosyan A, Falk M, Kajiyama MCC, Jundt DH, Buse K, Fejer MM (2011) Optical loss mechanisms in magnesium-doped lithium niobate crystals in the 300 to 2950 Nm wavelength range. In: Advances in optical materials, AIThE3. OSA, Istanbul. https://doi.org/10.1364/AIOM.2011.AIThE3
21. Zhenyu Z, Bo W, Nianmin Z, Chaoge X (2014) High-efficiency super-smooth chemical mechanical polishing method for lithium niobate crystal (China: Publication of CN103978406A) Application CN201410197096.5A (2014). Application publication date 13 Aug 2014
22. Meyn JP, Klein ME, Woll D, Wallenstein R, Rytz D (1999) Periodically poled potassium niobate for second-harmonic generation at 463 nm. Opt Lett 24(16):1154–1156
23. Uebernickel M, Fiebig C, Blume G, Paschke K, Eppich B, Güther R, Erbert G (2008) 400 mW and 16.5% wavelength conversion efficiency at 488 nm using a diode laser and a PPLN crystal in single pass configuration. Appl Phys B 93:823–827. https://doi.org/10.1007/s00340-008-3235-8
24. Rao A, Malinowski M, Honardoost A, Talukder JR, Rabiei P, Delfyett P, Fathpour S (2016) Second-harmonic generation in periodically-poled thin film lithium niobate wafer-bonded on silicon. Opt Express 24(26):29941–47. https://doi.org/10.1364/OE.24.029941
25. Kaushal H, Kaddoum G (2017) Applications of lasers for tactical military operations. IEEE Access 5:20736–20753
26. Peng Q, Juzeniene A, Chen J, Svaasand LO, Warloe T, Giercksky K-E, Moan J (2008) Lasers in medicine. Rep Progr Phys 71:056701